UCLA
UCLA Previously Published Works

Title

How Brine Composition Affects Fly Ash Reactions: The Influence of (Cat-, An-)ion Type

Permalink

https://escholarship.org/uc/item/2t939172

Journal

Advances in Civil Engineering Materials, 11(2)

ISSN

Authors

Collin, Marie
Prentice, Dale P
Arnold, Ross A
et al.

Publication Date

2022-11-28

DOI

Copyright Information

Peer reviewed

1
2 # How brine composition affects fly ash reactions: the influence of (cat-, an-)ion type
3
4 *Marie Collin ([1,2]), Dale P. Prentice ([1,2]), Ross A. Arnold ([1,2]), Kirk Ellison ([3]), Dante A. Simonetti*
5 *([2,4]), Gaurav N. Sant ([1,2,5,6])*
6
7 **ABSTRACT**
8 Hypersaline brines can be solidified and stabilized via the hydraulic and pozzolanic reactions
9 between fly ash(es) and calcium-based additives. While recent work has examined fly ash
10 reactivity in single-salt ("simple") hypersaline brines (ionic strength, I_m > 1 mol/L), the effects of
11 mixed-salt solutions on fly ash reactivity remain unclear. Herein, the reactivity of a Class C (CaO-
12 rich) or Class F (CaO-poor) fly ash mixture with $Ca(OH)_2$ is reacted in NaCl, $CaCl_2$, $MgCl_2$, and/or
13 Na_2SO_4-bearing solutions, for $1.5 \leq I_m \leq 2.25$ mol/L, from 1-week until 24-weeks. Expectedly,
14 sulfate anions promote the formation of sulfate phases (i.e., ettringite, monosulfoaluminate, U-
15 phase), while chloride anions induce the formation of Cl-AFm compounds (i.e., Kuzel's and
16 Friedel's salt). While the Class C fly ash's reactivity is similar across different anions (for a fixed
17 cation, and I_m), Class F fly ash shows a small change in reactivity depending on the anion
18 present. NaCl suppresses (Class C and Class F) fly ash reactivity by up to 30% as compared to
19 neat $CaCl_2$ and $MgCl_2$-based brines. Thermodynamic modeling reveals that NaCl induces a
20 considerable increase in pH – up to 13.7, where many hydrated phases of interest cease to be
21 the major phase expected – as compared to $CaCl_2$ and $MgCl_2$ brines (pH < 13). In a mixed-salt
22 brines, anion immobilization is competitive: sulfate achieves a greater level of incorporation
23 into the hydrates, as compared to chloride. These results offer new understanding of how the
24 brine composition affects solidification and stabilization, and thereby yield new insight into
25 improved approaches for wastewater disposal.
26
27 **Keywords:** Fly ash; hypersaline brine; solidification and stabilization; thermodynamic modeling;
28 chemical reactivity
29
30 **INTRODUCTION AND BACKGROUND**
31 Diverse sectors are working to fulfill zero-liquid discharge (ZLD) guidelines. Liquid waste streams
32 from agriculture, industry, mining, municipal, electricity generation, and produced water can
33 contain high levels of dissolved salts (0-to-5 mol/L of total dissolved solids: TDS).[1–5] Depending
34 on the waste stream type, these salts may include alkali and alkaline-earth cations, halide

[1] Laboratory for the Chemistry of Construction Materials (LC[2]), Department of Civil and Environmental Engineering, University of California, Los Angeles, CA, USA
[2] Institute for Carbon Management, University of California, Los Angeles, CA, USA
[3] Electric Power Research Institute, Charlotte, NC 28262, USA
[4] Department of Chemical and Biomolecular Engineering, University of California, Los Angeles, CA, USA
[5] Department of Materials Science and Engineering, University of California, Los Angeles, CA, USA
[6] California Nanosystems Institute (CNSI), University of California, Los Angeles, CA, USA

Corresponding authors: M. Collin (mariecollin03@ucla.edu) and G. Sant (Email: gsant@ucla.edu)

35 anions, as well as heavy metals. While multiple approaches have been developed to
36 significantly reduce the volume of liquid waste produced and to maximize water recycling, the
37 hypersaline solutions that are left behind – referred to as brines hereafter due to their high salt
38 content (ionic strength, I_m > 1 mol/L) – requires further treatment to fulfill ZLD guidelines.[1–5]
39
40 Solidification and stabilization (S&S) processes ensure the safe disposal of wastewaters by their
41 encapsulation in a solid matrix.[6,7] Here, the brine reacts with a binder to form a cemented solid
42 that retains the salts originally present in the brine.[6,7] The salts may be trapped by sorption
43 and/or by structural incorporation into the hydrated phases, [8–10], or by their precipitation (e.g.,
44 for heavy metals).[11] Additionally, the physical solidification of the cementitious matrix results in
45 the formation of a solid with a low porosity and low permeability, which reduces the transport
46 propensity of the contaminants.[12] Diverse cementitious binder formulations have been
47 considered for S&S applications.[13,14] A common cement replacement material, fly ash – which is
48 a co-product of coal combustion – is of particular interest. Fly ashes feature: (1) low-cost, and
49 (2) a low(er)-carbon footprint as compared to Ordinary Portland Cement (OPC). When a fly ash
50 is mixed with a calcium-containing additive (e.g., lime and/or various types of cement) and
51 water, the resulting pozzolanic reaction produces a cemented solid composed of calcium-
52 silicate-hydrates (C-S-H); e.g., similar to those formed during OPC hydration.[6,7,13] Using a large
53 fraction of fly ash and a low fraction of Ca-rich additive thus presents advantages in terms of
54 both cost and CO_2-footprint.[15,16]
55
56 A well-performing binder immobilizes dissolved species present in the brine.[6,13,16] Most brines
57 contain significant level of cations (sodium, calcium, magnesium, etc.) and anions (chloride,
58 sulfate, etc.), as well as heavy metals (e.g., selenium). Depending on the waste stream
59 considered, their SO_4^{2-} and Cl^- contents may vary significantly.[1–5] Both SO_4^{2-} and Cl^- strongly
60 affect the phase assemblage that forms due to their capacity for uptake in the Al_2O_3-Fe_2O_3-
61 mono and -tri phases (AFm and AFt, respectively), as well as other layered double hydroxides
62 (LDHs; i.e., hydrotalcite compounds). SO_4^{2-} is incorporated in ettringite (an AFt phase of general
63 formula $Ca_6Al_2(SO_4)_3(OH)_{12}\cdot26H_2O$) and/or monosulfoaluminate (an AFm phase of general
64 formula $Ca_4Al_2(SO_4)(OH)_{12}\cdot6H_2O$) depending on the SO_4^{2-}/Al ratio of the system.[17–19] Similarly,
65 Cl^- is typically incorporated in Kuzel's salt ($Ca_2Al(OH)_6[Cl, SO_4, OH]\cdot2H_2O$) and/or Friedel's salt
66 ($Ca_2Al(OH)_6[Cl,OH]\cdot2H_2O$), both of which will be referred to as "Cl-AFm phases" hereafter.[20–24]
67 Additionally, Cl^- might physisorb onto the C-S-H phases.[25–27] Cations may physisorb, or be
68 incorporated in the hydrated phases. For example, while Ca^{2+} is incorporated in the AFm and/or
69 AFt phases, as well as in C-S-H, Na^+ which is often present in abundance in a brine is typically
70 only physisorbed or remains mobile in the pore solution. The more consequential uptake of
71 anions as compared to cations results in the formation of OH^- anions to maintain
72 electroneutrality of the solution. This can result in a strong increase in the solution pH as anions
73 in the brine (e.g., Cl^-) are taken up into the solid phases.[28]
74
75 Because of differences in the solution chemistry (brine composition), the fly ash composition,
76 and the solid hydrates formed, the fly ash's degree of reaction can vary significantly. A previous
77 study showed that increasing Class F fly ash reactivity was observed with increasing NaCl and
78 $CaCl_2$ concentrations, although the effect of the latter is more pronounced than the former.[28] In

79   contrast, while high $CaCl_2$ concentrations resulted in enhanced Class C fly ash reactivity, NaCl
80   was shown to strongly inhibit Class C fly ash reactivity since the pore solution pH exceeded the
81   stability limits such that the persistence of the Cl-AFm phases was compromised.[28] But, this
82   prior study did not assess: (1) If the effect of Na^+ on pH amplification of the pore solution is
83   similar if SO_4^{2-} is the predominant anion (i.e., rather than Cl^-)?, (2) How other cations (e.g. Mg^{2+})
84   result in differences in hydrate composition, and solution chemistry vis-à-vis Na^+ and Ca^{2+}?, and
85   (3) How is fly ash reactivity altered in mixed-salt brines; i.e., rather than single-salt 'model'
86   brines?[28] With this focus in mind, this work examines the reactions of a Ca-rich (Class C) and a
87   Ca-poor (Class F) fly ash in mixed-ion/salt brines. Special attention is paid to assess the
88   evolution of the solid phase assemblages and fly using an experimental and thermodynamic
89   modeling approach. The outcomes provide new insights on the effects of the cations and
90   anions present in mixed-salt brines to ensure optimal brine encapsulation.
91
92   **MATERIALS AND METHODS**
93   *Raw material characterization*
94   A Class C and a Class F fly ash as detailed in Collin et al.,[28] were used herein. Their bulk oxide
95   composition is detailed in Table 1. The particle size distribution of both Class C and Class F fly
96   ash were measured by laser scattering (Beckman Coulter light scattering analyzer LS13-320)
97   using isopropanol and sonication for optimal particle dispersion. The results of the
98   measurement are shown in Table 1.
99

Table 1. The simple oxide compositions of the Class C and the Class F fly ash, including both crystalline and amorphous phases, as measured by X-ray fluorescence (mass %). The particle size distribution results, as measured by laser scattering.

Bulk oxide compositions (mass %)		
	Class C	**Class F**
CaO	28.0	4.0
MgO	7.2	0.9
Al_2O_3	18.5	20.7
SiO_2	32.1	52.0
SO_3	3.0	0.8
Fe_2O_3	5.3	14.6
Na_2O	1.8	1.4
K_2O	0.4	2.4
Others	3.7	3.2
Total	100.0	100.0
Particle size distribution (µm)		
	Class C	**Class F**
d_{10} value	0.1	0.2
d_{50} value	1.3	2.7

d_{90} value	7.4	14.3

100

101   Each fly ash was embedded in epoxy (Epotek 353ND) following the protocol of Chancey et al.,[29]
102   and then polished using sequentially finer grades of SiC sandpaper (grit numbers 400, 600, 800,
103   and 1200) and sequentially finer grades of diamond paste (6, 3, and 1 µm). The samples were
104   analyzed using a Nova NanoSEM™ scanning electron microscope (SEM) equipped with an
105   Energy-dispersive X-ray spectroscopy (EDS) detector. The microscope was operated at 10 kV
106   accelerating voltage and 6 mm working distance. The acquisition and data treatment was
107   performed following a protocol similar to that of Durdziński et al.[30] Briefly, a magnification of
108   200 and an image resolution of 1024 × 768 were selected. EDS elemental mapping was carried
109   out using an EDS count rate >15000 and a dead time below 30%. The fastest dwell time (50 µs)
110   was selected to reduce sample damage and to allow for a high number of scans within the time
111   frame of analysis. In total, 10 frames per samples were analyzed, allowing for the analysis of
112   more than 20,000 discrete particles. The count-maps were automatically converted into atomic
113   percentage-maps. The total acquisition and conversion time was estimated at 11 h per sample.

114

115   The compositional partitioning of the particles within the Ca-Al-Si (CAS) ternary system is
116   plotted in Figure 1 for both Class C (Figure 1a) and Class F fly ash (Figure 1b). The fly ash
117   composition was further separated into four categories (1 = silicate, 2 = Ca-silicate, 3 = Al-
118   silicate and 4 = Ca-Al-silicate) following the segmentation criteria proposed by Durdziński et
119   al.[30] The resulting repartitioning is detailed in Table 2. As expected, the Class F fly ash's
120   composition repartition is narrow and mostly centered around Al-silicates, and silicates to a
121   lesser extent.[30,31] In contrast, the Class C fly ash's composition repartition is well distributed
122   within the 4 types of silicates, as seen previously.[30,31] The average composition of the four
123   phases, calculated for both Class C and Class F, were found to be similar within error to that
124   calculated by Durdziński et al.[30]. While the segmentation criteria exclude some particles/areas
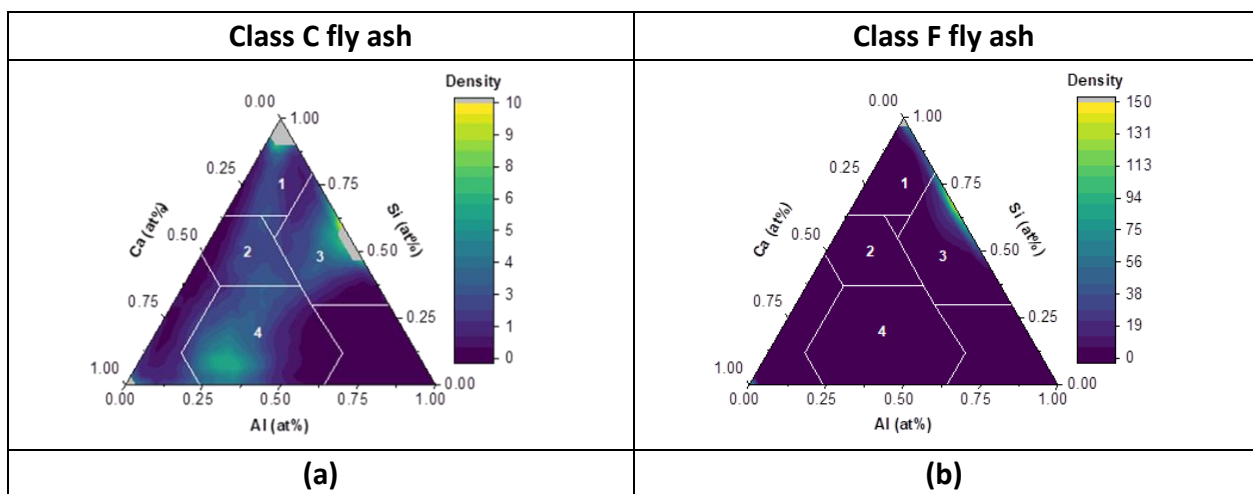125   (Figure 1), the exclusions represent <4% of the total population (see Table 2).

126

Class C fly ash	Class F fly ash
(a)	**(b)**

Figure 1. Al-Si-Ca ternary density plot (in atom %): **(a)** Class C and **(b)** Class F fly ash. The grey areas encompass high intensity area and are excluded to allow for better visualization of the other phases. White contours show the segmentation criteria as detailed by Durdziński et al.[30]

127

Table 2. A comparison of the four-phase populations that represent the amorphous content of the Class C and Class F fly ashes (volume fraction [%] based on the total population).					
	1 – Silicate	**2 – Ca-silicate**	**3 – Al-silicate**	**4 – Ca-Al-silicate**	**Others**
Class C	27.21	10.19	26.25	32.39	3.96
Class F	23.79	1.23	71.50	0.82	2.66

128

129 Simulated brines were prepared by dissolving analytical reagent (AR) grade NaCl, CaCl$_2$·2H$_2$O,
130 MgCl$_2$·6H$_2$O, and/or Na$_2$SO$_4$ in deionized water (DIW) at room temperature under agitation to
131 obtain single-salt or mixed-salt brines as detailed in Table 3. Overall, an ionic strength of
132 1.5 mol/L was targeted for the single- and mixed-salt brines. However, the mixed NaCl + Na$_2$SO$_4$
133 brine's ionic strength (2.25 mol/L) is higher due to the divalent sulfate anion's contribution.

134

Table 3. The ionic compositions of the seven simulated brines studied herein.					
Brine type	**Salt concentration (mol/L)**				**Total ionic strength (mol/L)**
	NaCl	**CaCl$_2$**	**MgCl$_2$**	**Na$_2$SO$_4$**	
NaCl	1.5	-	-	-	1.5
CaCl$_2$	-	0.75	-	-	1.5
MgCl$_2$	-	-	0.75	-	1.5
Na$_2$SO$_4$	-	-	-	0.75	1.5
NaCl + CaCl$_2$	0.75	0.375	-	-	1.5
CaCl$_2$ + MgCl$_2$	-	0.375	0.375	-	1.5
NaCl + Na$_2$SO$_4$	0.75	-	-	0.75	2.25

135

136 Cementitious formulations were prepared by combining 55 mass % of fly ash, 10 mass % of
137 Ca(OH)$_2$ (>95% purity) and 35 mass % of brine (i.e., a liquid to solid ratio of 0.54). The
138 formulations were mixed for 45 s at 270 rpm and 1 min at 480 rpm at room temperature using
139 a high-shear immersion mixer. The pastes were poured in hermetically sealed plastic containers
140 and placed in temperature regulated chamber at 25 °C. Thereafter, samples were periodically
141 retrieved (after 1-week, 6-weeks, 12-weeks and 24-weeks of reaction), crushed to a size of <10
142 mm and immediately immersed in isopropanol (IPA) for a week to arrest any further reaction.[32]
143 The samples were then dried under vacuum for an additional week, following which they were
144 crushed, milled using an agate pestle and mortar and then sieved through a 300 μm sieve prior
145 to additional characterization.

146

147 *Cementitious material characterization*
148 *Thermogravimetric analysis*: Thermogravimetric analysis (TGA) was performed using a Perkin
149 Elmer STA 8000 under a flow of ultra-high purity nitrogen using aluminum oxide crucible. A
150 heating ramp of 10 °C min^{-1} was used between 35 and 950 °C, after 5 min equilibration at 35 °C.
151 The mass loss (TG) and the derivative mass loss (DTG) were both used to quantify the

152   portlandite content, and the Cl-AFm hydrated phases which decompose in the temperature
153   between ≈250-to-430 °C.[33,34]
154
155   *X-Ray diffraction:* XRD analysis was performed using a PANalytical X'PertPro diffractometer (θ-θ
156   configuration, Cu-Kα radiation, λ = 1.54 Å) on powder samples containing 10 mass % ZnO
157   (99.99 mass % purity). The scans were acquired between 5° and 70° with a step-size of 0.02°
158   using an X'Celerator 2 detector. In general, powdered samples were placed in the sample
159   holder and their surfaces gently textured to minimize the potential for preferred orientation.
160   Rietveld refinement of the samples was performed using Profex/BGMN software.[35–37] The
161   following hydrated phases were identified: ettringite (ICSD #16045), monosulfoaluminate (ICSD
162   #100138), a magnesium-aluminum hydrotalcite-like phase (referred to as hydrotalcite,
163   hereafter, PDF #00-014-0525), katoite (ICSD #34227), Kuzel's salt (PDF #00-019-0203), Friedel's
164   salt (ICSD #62363), strätlingite (PDF #29-0285), and the U-phase whose peak position's
165   correspond to that observed by Li et al.[38]
166
167   *Infrared spectroscopy:* Solid-state attenuated total reflection Fourier-transform infrared
168   spectroscopy (ATR-FTIR) was performed using a Spectrum Two FT-IR Spectrometer (Perkin
169   Elmer). The powdered samples were pressed using around 90 N of force onto a diamond/ZnSe
170   composite crystal to ensure good contact and generate total internal reflection. The spectra
171   reported herein were obtained by averaging 4 scans over the wavenumber range of 4000-to-
172   400 cm^{-1} at a resolution of 1 cm^{-1}.
173
174   *Thermodynamic modeling*: Thermodynamic modeling was carried out using GEM-Selektor v.3.6
175   (GEMS)[39,40] which incorporates the slop98.dat and Cemdata18 thermodynamic databases.[41–45]
176   To represent the non-ideality of the solutions, the activity coefficients were calculated using the
177   Truesdell-Jones extension to the Debye-Hückel equation:[46]

$$\log_{10}\gamma_i = \frac{-A_\gamma z_i^2 \sqrt{I}}{1 + \dot{a}B_\gamma \sqrt{I}} + b_\gamma I + \log_{10}\frac{X_{jw}}{X_w} \qquad \text{Equation (1)}$$

178   where, γ_i is the activity coefficient and z_i the charge of the ith aqueous species, A_γ and B_γ are
179   temperature and pressure dependent coefficients, X_{jw} is the molar quantity of water, X_w is the
180   total molar amount of the aqueous phase, and I is the molal ionic strength. A common ion size
181   parameter (a = 3.72 Å) and a short-range interaction parameter (b_γ = 0.64 kg mol^{-1}) were
182   used, treating NaCl as the background electrolyte.[46,47] The system modelled (55 g of fly ash,
183   10 g of portlandite, and 35 g of brine) is equivalent to that studied experimentally. The ionic
184   strength I_m of the modeled systems was chosen to range from 0.05 (DI-water) to 2.5 mol/L
185   ($MgCl_2$ and $CaCl_2$ systems). Conversely, while the limit of applicability of Equation (1) is fixed at
186   around 2 mol/L, previous comparisons of ion activities determined using Pitzer's equations and
187   Equation (1) for simple Ca^{2+}-, Na^+-, and Cl^--containing systems yields results within ±30% for I_m <
188   4 mol/L.[13,48,49] Given that I_m < 2.5 mol/L for all solution compositions considered herein, while
189   the quantitative accuracy of the predictions of phase equilibria would degrade for I_m > 2 mol/L,
190   qualitative indicators (e.g., the types, and relative abundance of phases formed) would
191   nevertheless continue to be relevant to the systems studied. As such, some uncertainty is
192   expected in the outputs of the simulations performed at the highest ionic strengths.[39,49]

193
194 All phases used for the simulation, and to infer the degree of reaction of the fly ashes are
195 included in the slop98.dat and Cemdata18 thermodynamic databases.[41–45] However, the U-
196 phase is not currently represented in these databases.[50,51] Therefore, the U-phase's properties
197 were estimated based on an additive method as detailed by Blanc et al,[52] Hazen,[53] and Chermak
198 and Rimstidt.[54] Briefly, the thermodynamic properties of structurally relevant hydrated
199 components of the U-phase such as: $NaOH$, $Ca(OH)_2$, $CaSO_4.H_2O$, $Al(OH)_3$, and H_2O were
200 estimated from the thermodynamic properties of a selection of structurally and chemically
201 similar phases from the slop98.dat, the Cemdata18, and the Zeo19 thermodynamic
202 databases.[41–45,55] The Gibbs energy of formation ($\Delta_f G^{\circ}_{298}$), enthalpy of formation
203 ($\Delta_f H^{\circ}_{298}$),entropy (S°_{298}), and heat capacity (Cp°_{298}) of the U-phase (Table 4) were refined based
204 on the properties of the selected minerals. The molar volume (V°) was determined based on the
205 U-phase's molar mass given the linear relationship observed between the molar mass and the
206 molar volume of the selected minerals.
207

Table 4. The thermodynamic properties of the U-phase as used in the GEMS simulations.					
Chemical Formula (Dosch et al.[56])	**V°**	$\Delta_f G^{\circ}_{298}$	$\Delta_f H^{\circ}_{298}$	S°_{298}	Cp°_{298}
	(cm³/mol)	(kJ/mol)	(kJ/mol)	(J/mol/K)	(J/mol/K)
$4CaO·0.9Al_2O_3·1.1SO_3·0.5Na_2O·16H_2O$	34.86	-8936.34	-9467.51	968.16	1081.58

208
209 The fly ashes are considered to show fractional reactivity based on: (a) the lack of reaction of
210 the insoluble crystalline phases (e.g., quartz), (b) incomplete reaction of some partially soluble
211 crystalline and amorphous phases, and (c) complete consumption of the more-reactive
212 crystalline (e.g., $CaSO_4$) phases.[28] The dissolution behavior of the amorphous phase was
213 estimated from the dissolution behavior of the four silicate phases making up more than 96% of
214 the amorphous content of the fly ash (Figure 1 and Table 2). The dissolution behavior of each
215 silicate phase as a function of the fly ash degree of reaction was calculated from the silicate
216 phases unreacted volume fraction evolution over time, as observed by Durdziński et al.[30], and
217 fitted using a quadratic equation (Figure 2a). The dissolution behavior of each major (Si, Al, Ca)
218 and minor (Fe, Na, K and S) element was then inferred for all the silicate phases using the
219 calculated quadratic equations, the silicate phases repartition (Table 2), and the silicate phases
220 average composition.[30] The cumulative dissolution from the four phases was used to develop
221 element specific equations estimating the elemental dissolution as a function of the fly ash
222 degree of reaction. Al dissolution behavior calculation is provided as an example for Class C
223 (Figure 2b) and Class F fly ash (Figure 2c), showing (1) the contribution of each silicate phases
224 estimated from Figure 2a, and (2) the cumulative dissolution used to extract the dissolution
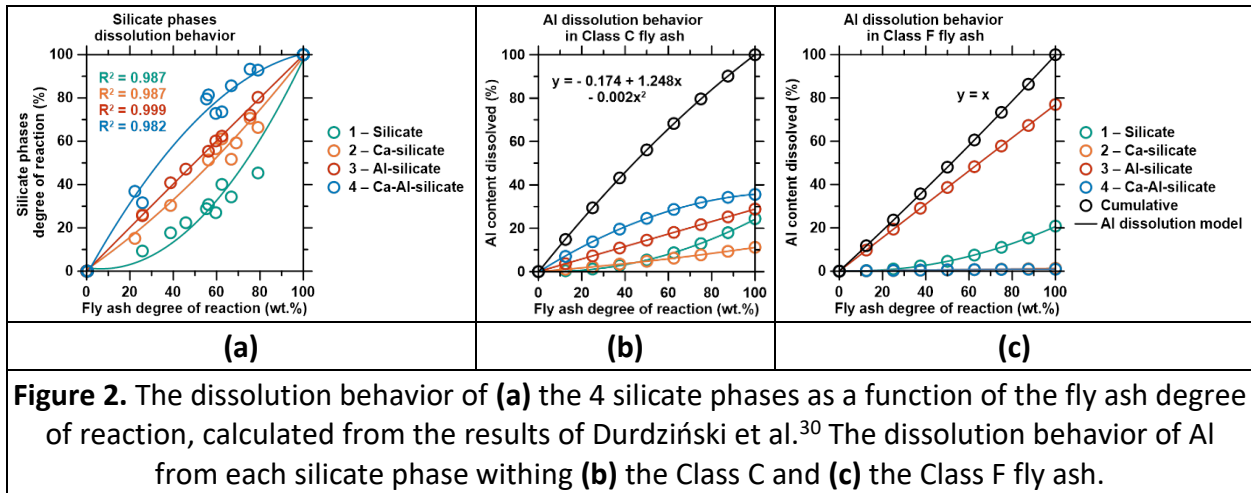225 models of Al for Class C and Class F fly ash.
226

Figure 2. The dissolution behavior of **(a)** the 4 silicate phases as a function of the fly ash degree of reaction, calculated from the results of Durdziński et al.[30] The dissolution behavior of Al from each silicate phase withing **(b)** the Class C and **(c)** the Class F fly ash.

227

228   From this assessment, it is inferred that the dissolution of the Class C fly ash is not congruent,
229   showing faster Al, Ca, and Mg release, and delayed Si release (Figure 3a and b). Quadratic
230   equations were developed for these four elements that exhibit incongruent behavior. The
231   dissolution of the other (minor) elements (Fe, Na, K and S) is nearly congruent, and is thus
232   modeled using a linear function. For the Class F fly ash (Figure 3c and d), the dissolution of all
233   elements (Al, Ca, Fe, Mg, Na, K, and S) except Si is near-congruent, while Si-dissolution follows
234   an incongruent/quadratic dissolution response. This approach of applying
235   congruent/incongruent dissolution, as appropriate to the phase of interest, significantly
236   improves the simulation of phase assemblages and phase ratios as compared to uniform
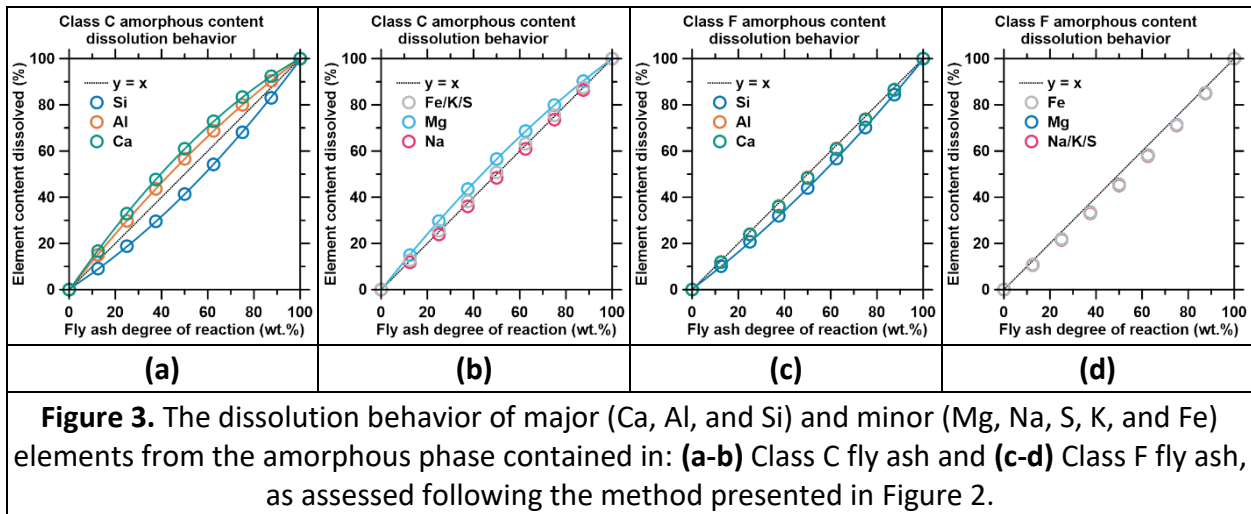237   congruency assumptions.[28]

238

Figure 3. The dissolution behavior of major (Ca, Al, and Si) and minor (Mg, Na, S, K, and Fe) elements from the amorphous phase contained in: **(a-b)** Class C fly ash and **(c-d)** Class F fly ash, as assessed following the method presented in Figure 2.

239

240   Finally, the degree of fly ash reaction at 7 to 168 days of reaction was inferred by analyzing
241   when the mass ratio of the crystalline phases (e.g., portlandite CH: $Ca(OH)_2$) is equal to unity;
242   i.e., when the modeled quantity of the phases is equal to its content as established by
243   experimental, i.e., TGA and/or XRD assessments (e.g., when $CH_m/CH_e \approx 1$, where the subscripts
244   'm' and 'e' indicate modeled and experimental assessments).

245

246 **RESULTS AND DISCUSSION**

247 *Single-salt brines*: Both Class C and Class F fly ash hydration in DIW, NaCl, or Na$_2$SO$_4$ brine result

248 in the formation of vastly different hydrated phase assemblages after 24-weeks of reaction

249 (Figure 4a and c, respectively). The Class C fly ash hydrated in DIW features

250 monosulfoaluminate (with SO$_4^{2-}$ contributed by the dissolution of CaSO$_4$ from the fly ash),

251 hydrotalcite, katoite, and traces of strätlingite. The introduction of Na$_2$SO$_4$ destabilizes katoite

252 and monosulfoaluminate resulting in the formation of ettringite and the U-phase (a Na-

253 containing AFm phase of formula 4CaO·0.9Al$_2$O$_3$·1.1SO$_3$·0.5Na$_2$O·16H$_2$O)[38,56–58] – while the

254 formation of strätlingite is unaffected. In contrast, introducing NaCl destabilizes all the phases

255 otherwise formed in DIW, and only Friedel's salt, a Cl$^-$-containing AFm phase forms instead.

256 Interestingly, if NaCl is replaced by CaCl$_2$ or MgCl$_2$ at equivalent anionic concentration,

257 strätlingite persists alongside Friedel's salt, Kuzel's salt and ettringite, showing again that alkali

258 and alkaline-earth cations differently affect the stable phase assemblage (Figure 4b). The Class

259 F fly ash system in DIW forms ettringite and monosulfoaluminate due to the fast dissolution of

260 CaSO$_4$ from the Class F fly ash (Figure 4c). In the presence of Na$_2$SO$_4$, the increased SO$_4^{2-}$

261 content enhances the formation of ettringite at the expense of monosulfoaluminate (SO$_4^{2-}$-

262 AFm). In contrast, in the presence of NaCl, all sulfate-bearing hydrated phases are replaced by

263 Friedel's salt. A similar phase assemblage as the NaCl system is observed in CaCl$_2$ or MgCl$_2$-

264 containing brine systems, although the Friedel's salt content is higher in these instances

265 compared to NaCl (Figure 4d and Figure S1), mainly due to differences in the pH of the pore

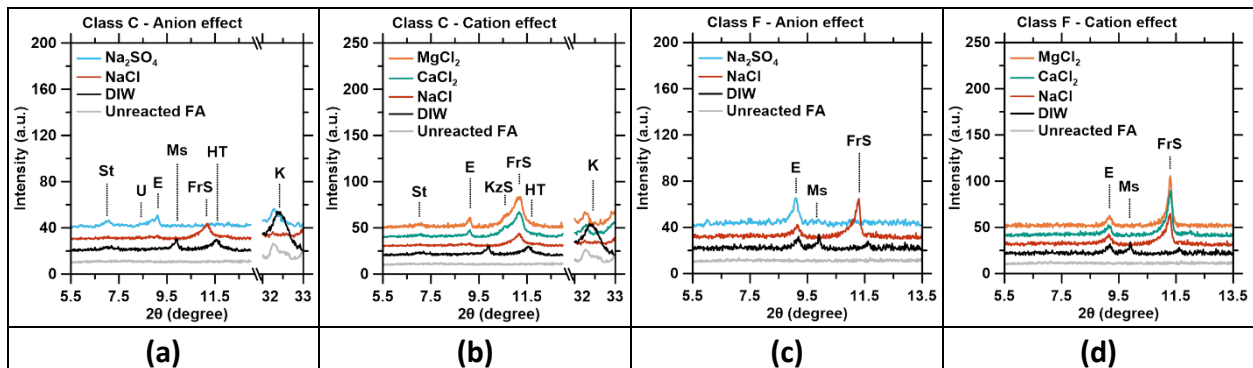266 solution, as will be discussed below.

267

(a) (b) (c) (d)

Figure 4. The hydrated assemblage – with a background subtraction – after 24-weeks of hydration at 25 °C for the Class C fly ash **(a)** in NaCl and Na$_2$SO$_4$ brines, and **(b)** in Cl$^-$-containing brines (NaCl, CaCl$_2$ or MgCl$_2$). Also shown is the Class F fly ash reacted **(c)** in NaCl and Na$_2$SO$_4$ brines, and **(d)** in Cl$^-$-containing brines (NaCl, CaCl$_2$ or MgCl$_2$). Here, E = ettringite, Ms = monosulfoaluminate, U = U-phase, FrS = Friedel's salt, KzS = Kuzel's salt, HT = hydrotalcite, St = strätlingite and K = katoite.

268

269 The differences between the hydrated phase assemblages of Class C and Class F fly ash across

270 all brine types is unsurprising on account of differences in their composition, and their

271 (differing) reactivity in different solution environments. The higher Ca content in Class C fly ash

272 renders its amorphous component far more reactive; due to the reduced rigidity of its atomic

273 network.[31,59,60] As a result, a Class C fly ash will release greater amounts of Ca, Si, and Al over
274 time as compared to a Class F fly ash. This results in a decrease of the (anion)/Al ratio which
275 allows for: (1) higher anion uptake, and (2) the formation of a larger quantity of hydrated
276 phases. In the presence of a Na_2SO_4 brine, for example, the formation of two SO_4^{2-}-bearing
277 phases (ettringite and the U-phase) and strätlingite is observed in the Class C system, while only
278 ettringite forms in the Class F system. In Cl^--containing brines, the higher reactivity of Class C fly
279 ash leads to the formation of multiple hydrated phases in addition to Cl-AFm compounds
280 (which forms in a larger quantity vis-à-vis the Class F fly ash system: see Figure S1), while in the
281 Class F fly ash system Friedel's salt is the major phase formed along with a minor amount of
282 ettringite.
283
284 Finally, as expected from the pozzolanic reaction between the fly ashes and portlandite, both
285 Class C and Class F fly ash hydration results in the formation of an amorphous calcium-silicate-
286 hydrate (C-S-H) phase, as attested by the IR spectra (Figure 5) showing a distinct peak around
287 960 cm^{-1}.[61] The peak position and shape suggest aluminum and magnesium incorporation.[61,62]
288 Overall, the C-S-H peak intensity does not significantly vary across all brine compositions
289 studied, indicating that the amount of C-S-H formed is similar across brine compositions. But,
290 the C-S-H peak position shifts to higher wavenumbers in $MgCl_2$ and $CaCl_2$ systems compared to
291 DIW, NaCl and Na_2SO_4, which suggest enhanced Ca^{2+} and Mg^{2+} incorporation in these systems
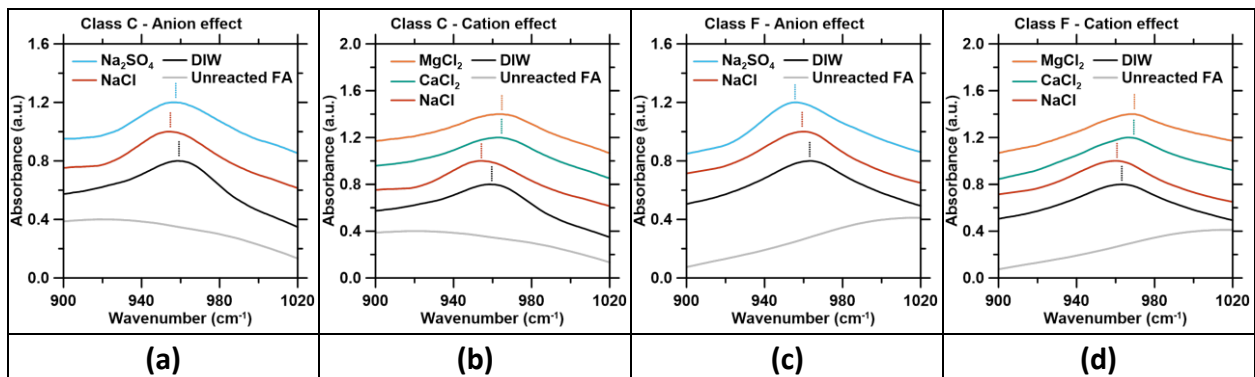292 indicative of a potentially greater Ca/Si and Mg/Ca ratios herein.[61,62]
293

Figure 5. C-S-H formation as observed from IR spectroscopy analysis after 168 days of hydration
at 25 °C of the Class C fly ash **(a)** in NaCl and Na_2SO_4 brines and **(b)** in Cl^--containing brines
(NaCl, $CaCl_2$ or $MgCl_2$), and the Class F fly ash **(c)** in NaCl and Na_2SO_4 brines and **(d)** in Cl^--
containing brines (NaCl, $CaCl_2$ or $MgCl_2$).

294
295 In general, the observed phase assemblages were successfully reproduced via thermodynamic
296 modeling. The modeled pore solution pH varied for Class C and Class F fly ashes (pH 12.9-13.9
297 for Class C fly ash, 12.0-13.8 for Class F fly ash) across the different brine compositions as
298 observed previously.[28] For example, Na^+ incorporation in hydrated phases that occurs to a level
299 inferior to that of its corresponding charge-balancing anion in the native brine was previously
300 shown to induce a strong increase in pH to ensure electrolytic charge compensation NaCl-
301 containing solutions.[28] The results displayed in Figure 6 demonstrate that a similar Na^+ effect is
302 observed in sulfate-containing brines. The effect is shown to be even stronger in sulfate-

303 containing brines compared to chlorine-containing brines due to: a) a higher extent of SO_4^{2-}
304 uptake (Figure S2), and b) the divalent nature of SO_4^{2-} compared to Cl^- that requires a larger
305 amount of OH^- formation to charge balance; resulting in higher pH. In contrast, alkaline-earth
306 cation-containing brines (Mg^{2+} and Ca^{2+}) show a lower pH compared to DIW system. This is
307 because, unlike Na^+, divalent cations are more extensively incorporated into the hydrated
308 phases, e.g., AFm and AFt (Ca^{2+} only) phases, and C-S-H (which incorporates both Mg^{2+} and
309 Ca^{2+}). The incorporation of cations to a level higher than that of their corresponding anions
310 induces the formation of H^+, resulting in an inferior pH vis-à-vis the DIW systems. It is worth
311 noting that, for the Class C fly ash, in DIW, and univalent cation brines the increase in pH after
312 7-days shows minimal changes thereafter (Figure 6). In contrast, the pH rises from 12.0 to 12.9
313 for systems containing Ca^{2+} and Mg^{2+}-based brines as phase formation and phase
314 transformations continue to occur up to around 80 days of reaction. In the case of the Class F
315 fly ash, the pH and phase assemblage evolve across brine compositions up to 6-weeks of
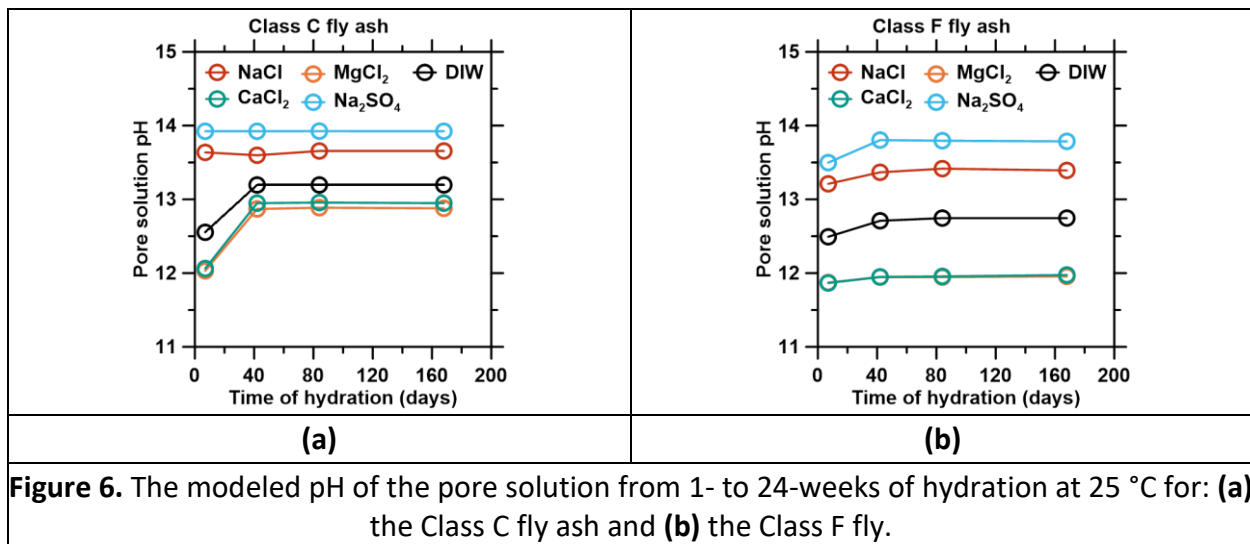316 reaction, after which they stabilize thereafter.
317

Figure 6. The modeled pH of the pore solution from 1- to 24-weeks of hydration at 25 °C for: **(a)** the Class C fly ash and **(b)** the Class F fly.

318
319 The systems showing the lowest cation incorporation (NaCl and Na_2SO_4) also showed (1) the
320 highest pore solution pH (Figure 6) and (2) the lowest amount of hydrated phase formation
321 (Figure 4 and Figure S1), indicating the smallest extent of fly ash reaction (Figure 7) as
322 compared to the systems with a lower pH (DIW, $CaCl_2$ and $MgCl_2$). This suggests that the high
323 pore solution pH (≥13.4) may limit the formation of SO_4^{2-}- and/or Cl^--containing hydrated
324 phases whose formation is consequent with fly ash reaction (dissolution). Additionally, it is
325 possible that the lower amount of readily available cations to form AFm and/or C-S-H also
326 further limit the fly ash reactivity. For the Class C fly ash, all systems are still in excess of
327 portlandite (Figure S3), and the reduced reactivity is thus more likely related to pore solution
328 pH differences. The formation of Cl^- or SO_4^{2-} containing AFm or AFt phases is detrimental to the
329 formation of other hydrated phases (e.g. Katoite) unless a high enough pore solution pH is
330 reached, as observed in a previous study.[28] As the amount of Cl^- or SO_4^{2-} containing AFm or AFt
331 starts being restricted by the high pH, the overall amount of hydrated phases formed in NaCl
332 and Na_2SO_4 is lower than (1) in DIW, and (2) in $CaCl_2$ and $MgCl_2$. Thus, both NaCl and Na_2SO_4

333   induce a strong decrease in the Class C fly ash's extent of reaction at longer reaction times
334   (Figure 7a). The Cl⁻-containing AFm and AFt formed in $CaCl_2$ and $MgCl_2$ are less constrained by
335   the pore solution pH, thus the amount of hydrated phases formed is equivalent to that formed
336   in DIW, resulting in a similar fly ash extent of reaction (Figure 7b). For Class F fly ash, Cl⁻ or SO_4^{2-}
337   containing AFm or AFt form in addition to the phases observed in DIW, thus, the reactivity in
338   brines is higher than in DIW regardless of the brine type (Figure 7c and d). The simultaneous
339   formation of Friedel's salt and ettringite leads to a slightly higher extent of fly ash reaction with
340   NaCl than with Na_2SO_4; in the latter case only ettringite formation occurs. This suggests that, for
341   a fixed anion content, the fly ash reactivity may vary as a function of the anion type. The
342   amount of Friedel's salt formed in NaCl is lower than in $CaCl_2$ and $MgCl_2$, either because of the
343   higher pore solution pH, and/or because the amount of Ca^{2+} available is more limited, resulting
344   in a lower fly ash extent of reaction at longer reaction time. Finally, it is interesting to observe
345   that most of the fly ash reactions takes place within the first 6-weeks of hydration, while little
346   increase in reaction is observed at later times (see Figure 7).
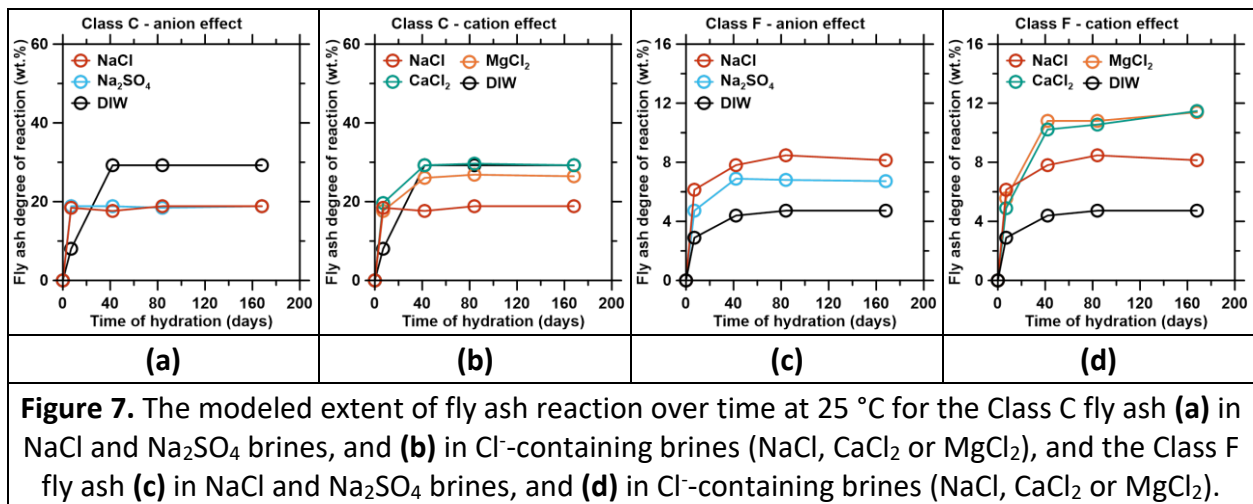347

(a)	**(b)**	**(c)**	**(d)**

Figure 7. The modeled extent of fly ash reaction over time at 25 °C for the Class C fly ash **(a)** in NaCl and Na_2SO_4 brines, and **(b)** in Cl⁻-containing brines (NaCl, $CaCl_2$ or $MgCl_2$), and the Class F fly ash **(c)** in NaCl and Na_2SO_4 brines, and **(d)** in Cl⁻-containing brines (NaCl, $CaCl_2$ or $MgCl_2$).

348
349   The results confirm that both the type of anions directly affect the phase assemblage; and the
350   extent and type of formation of the AFm and AFt phases. On account of the ability of OH⁻ or
351   CO_3^{2-} to also form AFm-phases, the phases that form are expected to correspond with the site-
352   occupation preferences of AFm (and AFt) phases.[63,64] While herein similar reactivity is observed
353   for the Class C fly ash across brine compositions, the results obtained for the Class F fly ash
354   suggest that, the anion(s) contained in the brine affect both the type and content of hydrated
355   phases that may form, and therefore affect the fly ash's reactivity. The cations – and more
356   specifically the alkaline-earth cations – can also be incorporated in the hydrated phases. This
357   can strongly influence the pore solution pH, which in turn significantly affects the amount and
358   the type of phases formed in correspondence with their pH-based solubility compared to other
359   hydrated phases. The cations consequently affect fly ash reactivity more noticeably than the
360   anions, following the order $Na^+ << Mg^{2+} \approx Ca^{2+}$. This suggests that, in general, divalent
361   (polyvalent) cations more strongly affect fly ash reactivity than univalent cations on account of
362   the incorporation of the former within hydrated phases; while the latter mostly display
363   reversible surface sorption behavior.

364

365   *Mixed brines*: The behavior of cations and anions was further assessed in mixed systems. First, a

366   mixed $NaCl/Na_2SO_4$ system was compared to the single-NaCl and Na_2SO_4 systems studied

367   above. For the Class C fly ash, the mixed-salt system's phase assemblage after 24-weeks of

368   reaction is an intermediate of the phase assemblages obtained in single salt systems (Figure

369   8a). Specifically, while the formation of ettringite and the U-phase is observed, as is the case in

370   the single Na_2SO_4 system, strätlingite is replaced by the formation of a small quantity of

371   Friedel's salt. For the Class F fly ash, the mixed-salt system phase assemblage after 168 days is

372   similar to the single-salt Na_2SO_4 system (Figure 8b): ettringite forms preferentially, and no

373   Friedel's salt formation is observed. The anions therefore show a competitive effect, with SO_4^{2-}

374   incorporation into ettringite prevailing above Cl^- incorporation into Friedel's salt. This is

375   explained by ettringite's low solubility, as attested by its solubility product (log K_{sp} = -44.9 at

376   room temperature)[65] which is substantially lower than that of Friedel's salt (log K_{sp} = -27-28 at

377   room temperature);[24,66] which explains why SO_4^{2-} incorporation prevails over Cl^- in the Class F

378   system. This competitive effect between Cl^- and SO_4^{2-} is less prevalent in the Class C system,

379   compared to the Class F system, due to (1) the Class C fly ash's higher degree of reaction –

380   which mobilizes Ca-in solution allowing for higher anion incorporation into the Ca-based

381   hydrated phases (Figure S2), and (2) Friedel salt's solubility being lower than that of strätlingite

382   (log K_{sp} = -20 at room temperature)[64] as a result of which Friedel's salt formation is preferred.

383

384   As a result of the competitive effect of the anions, the degree of reaction of Class F fly ash

385   (Figure 8d) in mixed-salt systems is similar to that of the single salt systems, despite the final

386   ionic strength being twice as high. A similar observation is made for Class C fly ash, despite

387   meaningful Cl^- and SO_4^{2-} incorporation, due to the destabilization of strätlingite by Friedel's salt.

388   These results suggest that the solubility and stability of the hydrated phases is more important

389   than the preference of anion incorporation into the hydrated phases. For example, competitive

390   uptake has been previously observed in AFm and Mg-Al-LDH phases.[67–69] And, while previous

391   studies have shown that for LDH phases, anion preference follows as Cl^- > NO_3^- > NO_2^- > CO_3^{2-} >

392   SO_4^{2-} > OH^-, likely for both ion exchange and ion incorporation,[68,70,71] herein SO_4^{2-} incorporation

393   is shown to dominate on account of ettringite having a solubility that is much lower than

394   Friedel's salt. This suggests that additional competitive effects could be observed if other anions

395   are present in the brine (e.g. CO_3^-, Br^-, F^-); as the presence of such anions could provoke the

396   formation of other hydrated phases that might preferentially form if their solubility is lower

397   than that of Friedel's salt and/or ettringite.[20]

398

399   In mixed-cation systems (i.e., mixed $NaCl/CaCl_2$ or mixed $CaCl_2/MgCl_2$ wherein $[Cl^-]$ = 1.5 mol/L),

400   the phase assemblage is observed to present a near-average of the single-salt phase

401   assemblages (see Figure 9). For example, the Class C systems display a phase assemblage for

402   the mixed $NaCl/CaCl_2$ brines (Figure 9a) that features the enhanced formation of Friedel's salt

403   and ettringite, while the formation of strätlingite and Kuzel's salt is suppressed. In contrast, the

404   phase assemblage resulting from mixed $CaCl_2/MgCl_2$ brine is equivalent to the phase

405   assemblage formed from the single-salt $CaCl_2$ and $MgCl_2$ brines (Figure 9b). In the Class F fly ash

406   system, reaction in a mixed $NaCl/CaCl_2$ brine result in the formation of ettringite and Friedel's

407   salt, similar to what is observed in single salt systems (Figure 9c). Here, the amount of Friedel's

408   salt formed is the arithmetic mean of that formed in the single salt systems (Figure S4). Finally,
409   as was the case for Class C fly ash, the phase assemblage resulting from mixed $CaCl_2$/$MgCl_2$
410   brine encapsulation is similar to the phase assemblage formed from single $CaCl_2$ or $MgCl_2$ brines
411   (Figure 9d). These results suggest that cations show an "additive effect", wherein the effect of
412   each cation can be summed, instead of a competitive effect where the effect of one cation
413   would prevail over the other. This assessment is further confirmed by the thermodynamic
414   modeling of the extent of fly ash reaction (Figure 9e to h): the extent of fly ash reaction in the
415   mixed-salts brines can be inferred from the single-salt brine systems by a "rule of mixtures"
416   type that is simply a function of the salt type and concentration:

417

$$DR_{\text{mixed brine}} = DR_{\text{DIW}} + \left[DR_{\text{single brine 1}} - DR_{\text{DIW}}\right] * \frac{[\text{salt 1}]_{\text{mixed brine}}}{[\text{salt 1}]_{\text{single brine 1}}}$$
$$+ \left[DR_{\text{single brine 2}} - DR_{\text{DIW}}\right] * \frac{[\text{salt 2}]_{\text{mixed brine}}}{[\text{salt 2}]_{\text{single brine 2}}} \qquad \text{Equation (2)}$$

418   In the case of mixed $CaCl_2$/$MgCl_2$ systems, the measured degree of reaction is equivalent to that
419   calculated from the single-salt $CaCl_2$ and $MgCl_2$ systems. And, in the mixed NaCl/$CaCl_2$ systems,
420   the degree of reaction is an average of that of the single NaCl and $CaCl_2$ systems, as the $CaCl_2$
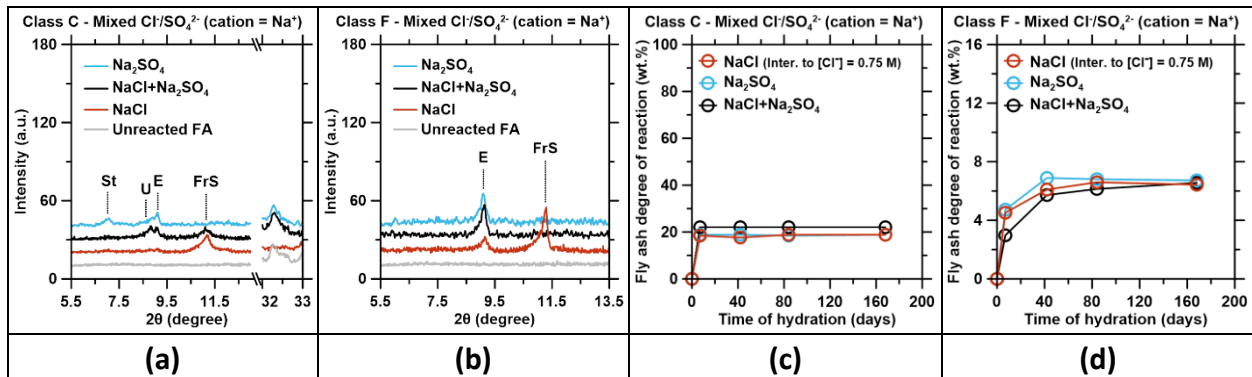421   system results in a higher extent of fly ash reaction than pure-NaCl system.

422

Figure 8. The phase assemblage – with background subtraction – after 24-weeks of reaction at 25 °C of **(a)** the Class C fly ash and **(b)** the Class F fly ash reacted in mixed-anion brines. The modeled degree of fly ash degree over time for **(c)** the Class C fly ash and **(d)** the Class F fly ash. Here, E = ettringite, U = U-phase, FrS = Friedel's salt, and St = strätlingite. Here, the NaCl system is interpolated to [Cl⁻] = 0.75 M based on previous observations showing (1) a plateau in the degree of fly ash reaction with increasing Cl⁻ concentration >0.5 M for Class C fly ash, and (2) a linear increase in the degree of fly ash reaction with increasing Cl⁻ concentration for the Class F fly ash.[72]

423

424   The prevailing pH of the pore solution as induced by the uptake of cations, or anions and the
425   corresponding need for electroneutrality (of the solution) is identified to be a predominant
426   factor that affects the extent of Class C fly ash reaction.[28,72] The observations related to the
427   mixed-brine systems further confirm that hypothesis. Class C fly ash reactions are shown to
428   cease when the pore solution pH exceeds 13.6, while systems reacting in less caustic solutions
429   are noted to continue reacting (Figure S5a). This suggests that reaction rate controls are

430   imposed in this case, not by the dissolution rate of the fly ash precursors, which is most often
431   rate limiting, but rather, the inability to preferentially form reaction products of interest in
432   these chemical environments. This indicates that: (1) pH ~ 13.6 corresponds to a limit for the Cl-
433   AFm phases preferential formation, and (2) said Cl-AFm preferential formation is a major
434   driving force for fly ash reaction, conceivably more so than the classical hydration/pozzolanic
435   reactions. A reduction in the extent of reaction with increasing pH is notable, as silicate
436   dissolution increases with increasing pH.[73–76] This highlights the fact that, although atypical in
437   most environments, in brine systems free of ordinary portland cement (OPC), hydrated phase
438   formation more prominently affects the extent of fly ash reacting than its own (silicate)
439   dissolution. The pH-effect on fly ash reaction is however less significant in the case of the Class
440   F fly ash because on account of a smaller amount of net-anion uptake from the brine, pH 13.6 is
441   not attained herein, as a result of which Class F reactivity, in general is higher in Cl⁻-containing
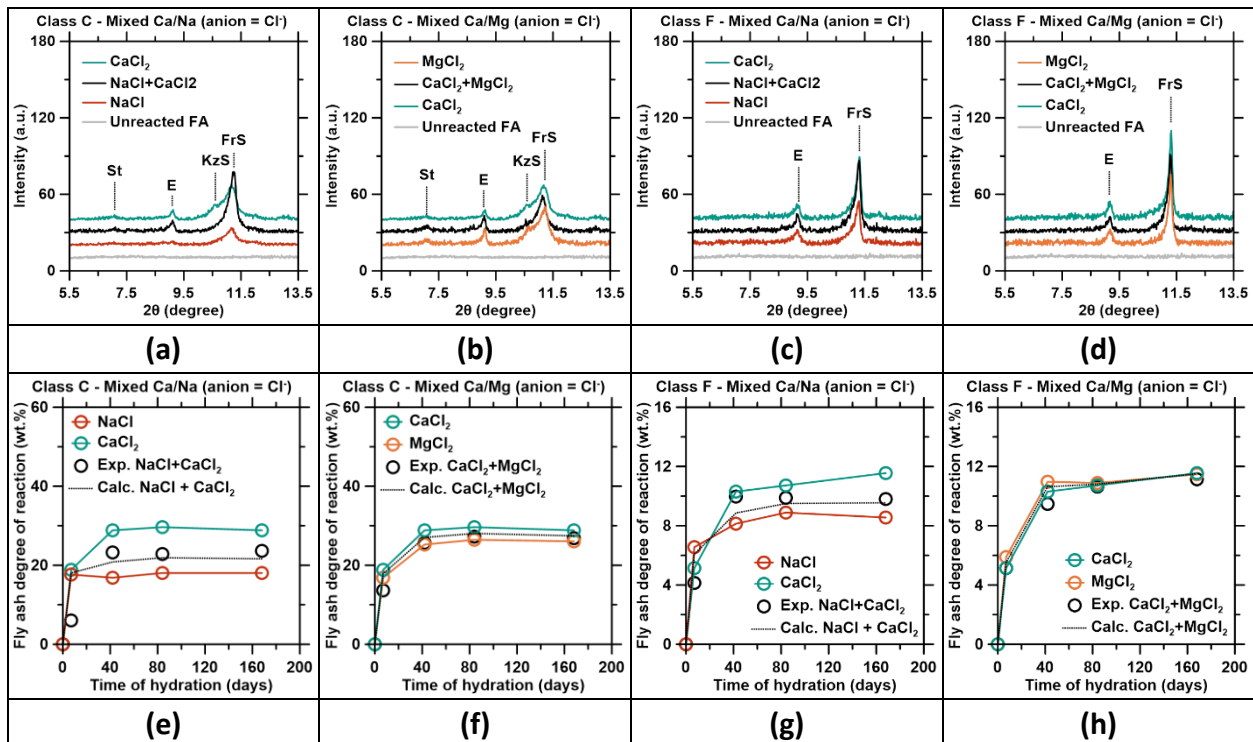442   brines than in DIW.

443

Figure 9. The phase assemblage and the extent of fly ash reaction after 24-weeks of reaction at 25 °C for the Class C fly ash reacting in **(a)** and **(e)** mixed $CaCl_2$ and NaCl brines and **(b)** and **(f)** mixed $CaCl_2$ and $MgCl_2$ brines, and for the Class F fly ash in **(c)** and **(g)** mixed $CaCl_2$ and NaCl brines and **(d)** and **(h)** mixed $CaCl_2$ and $MgCl_2$ brines. Here, E = ettringite, FrS = Friedel's salt, KzS = Kuzel's salt, and St = strätlingite.

444
445   It should be noted that, both in Cl⁻-containing and SO_4^{2-}-containing systems wherein the pH
446   does not meet or exceed the 13.6 threshold, the reaction of the fly ash diminishes once
447   strätlingite forms (Class C fly ash, Figure 4a and b), or after portlandite is consumed (Class F fly
448   ash, see Figure S6). This suggests that, for Class C fly ash, Cl-AFm and/or SO_4^{2-}-containing phase
449   formation is the driving force of the fly ash reactivity. Once these phases are destabilized,

450 resulting in the formation of strätlingite, the solution conditions shift sufficiently such that fly
451 ash reactions cease. For Class F fly ash, while the formation of Cl-AFm and/or SO_4^{2-}-containing
452 phases promotes fly ash reaction (as demonstrated by the increase in reactivity compared to
453 the DIW system), the pozzolanic reaction promotes ongoing Class F fly ash reaction. But once
454 the portlandite is consumed, the pozzolanic reaction, and consumption of fly ash both ceases.
455
456 **CONCLUSION**
457 The type and abundance of cations and anions in a brine is shows to significantly affect both the
458 nature of phase assemblage formed, and the extent of fly ash reaction; over 24-weeks of
459 reaction at 25 °C. The presence of sulfate anions promotes the formation of
460 monosulfoaluminate and the U-phase in the presence of a Class C fly ash, and additionally
461 ettringite in the presence of a Class F fly ash – as the dominant phases. In contrast, chloride
462 anions promote the formation of Friedel's and/or Kuzel's salt. While here, the extent of
463 reaction of the fly ashes is shown to be similar at an equimolar anion content; varying the
464 anions present alters the extent of fly ash reacted on account of the different hydrated phases
465 that may form. For example, NaCl, $CaCl_2$, and $MgCl_2$ containing brines all promote the
466 formation of Cl-AFm compounds. However, NaCl results in a reduced extent of fly ash reaction
467 for both Class C and Class F fly ashes as compared to divalent cation brines. This effect is
468 particularly notable for the Class C fly ash that shows an extent of reaction lower than that
469 observed in DIW, due to the pH of the pore solution exceeding 13.6; where Cl-AFm preferential
470 formation is compromised and which, in turn, halts ongoing fly ash reactions. These
471 observations thus suggest that the type of cation(s) is, both directly and indirectly, a main factor
472 of system reactivity, following the order $Na^+ << Mg^{2+} \approx Ca^{2+}$. When elevated pH is not the
473 limiting factor, Class C fly ash reactions are driven by Cl-AFm and/or SO_4^{2-}-containing phase
474 formation; unless strätlingite begins to form on account of the destabilization of the former
475 compounds. In the case of Class F fly ash, their reaction is affected by the pozzolanic reaction,
476 and a decrease of fly ash reactivity is observed once portlandite is consumed, whereby the
477 formation of C-S-H ceases.
478
479 In mixed-salt brines, the anions show a strong competitive effect where sulfate is preferentially
480 incorporated over chloride and is the dominant influence on fly ash reactivity. It is postulated
481 here that any type of anion that can occupy the interlayer positions of AFm and AFt phases
482 would display a similar competitive effect in relation to the interlayer site-occupation
483 preference for a given phase, and the relative solubility of the different phases; e.g., wherein
484 ettringite formation prevails above Friedel's salt, and Friedel's salt formation prevails above
485 strätlingite. The preferential incorporation order observed here ($SO_4^{2-} > Cl^-$) therefore differs
486 from that typically observed within a select AFm/LDH-type phase ($Cl^- > NO_3^- > NO_2^- > CO_3^{2-} >$
487 $SO_4^{2-} > OH^-$), on account of ettringite having a solubility that is much lower than Friedel's salt. In
488 contrast, the cations show an additive effect: the fly ash reactivity in the mixed-salt brines is an
489 average of that observed in the single-salt brines. Similar additive effect is expected across
490 diverse cation types, provided that their effect is similar to that of Na^+, Ca^{2+}, or Mg^{2+}. As such,
491 while the mixing of cations is less important from a disposal perspective, mixed anion brines
492 pose a problem, in that anion will preferentially be encapsulated. For example, sulfate- and
493 chloride-containing brines are not ideal: sulfate incorporation will supplant chloride

494 incorporation, which may enhance the potential of chloride release into the environment. New
495 understanding of this nature of both the additive and competitive effects of brine (ion)
496 components during encapsulation is crucial to enable enhanced and improved disposal of
497 wastewaters. These considerations will assist in fulfilling stringent regulatory standards and
498 reducing the risk of the release of contaminants into the surrounding environment.
499

500 **ACKNOWLEDGMENTS**
508

509 **REFERENCES**
510 1.   Borch, T. *et al.* National Alliance for Water Innovation (NAWI) Technology Roadmap:
511 Agriculture Sector. 150 (2021).
512 2.   Cath, T. *et al.* National Alliance for Water Innovation (NAWI) Technology Roadmap:
513 Resource Extraction Sector. 130 (2021).
514 3.   Cath, T. *et al.* National Alliance for Water Innovation (NAWI) Technology Roadmap:
515 Industrial Sector. 104 (2021).
516 4.   Childress, A. *et al.* National Alliance for Water Innovation (NAWI) Technology Roadmap:
517 Power Sector. 112 (2021).
518 5.   Giammar, D. *et al.* National Alliance for Water Innovation (NAWI) Technology Roadmap:
519 Municipal Sector. 114 (2021).
520 6.   Renew, J. E. *et al.* Immobilization of heavy metals by solidification/stabilization of co-
521 disposed flue gas desulfurization brine and coal fly ash. *Energy Fuels* **30**, 5042–5051 (2016).
522 7.   Huang, C.-H., Renew, J. E. & Wenlong Zhang, M. S. *Mineralogy optimization for metal*
523 *and chloride immobilization in co-disposed flue gas desulfurization brines and bituminous coal*
524 *fly ash*. 42 (2019).
525 8.   Gougar, M. L. D., Scheetz, B. E. & Roy, D. M. Ettringite and C-S-H Portland cement phases
526 for waste ion immobilization: A review. *Waste Management* **16**, 295–303 (1996).
527 9.   Piekkari, K., Ohenoja, K., Isteri, V., Tanskanen, P. & Illikainen, M. Immobilization of heavy
528 metals, selenate, and sulfate from a hazardous industrial side stream by using calcium
529 sulfoaluminate-belite cement. *Journal of Cleaner Production* **258**, 120560 (2020).
530 10.   Van Jaarsveld, J. G. S., Van Deventer, J. S. J. & Lorenzen, L. The potential use of
531 geopolymeric materials to immobilise toxic metals: Part I. Theory and applications. *Minerals*
532 *Engineering* **10**, 659–669 (1997).
533 11.   Glasser, F. P. Fundamental aspects of cement solidification and stabilisation. *Journal of*
534 *Hazardous Materials* **52**, 151–170 (1997).
535 12.   Renew, J. E. *et al.* Immobilization of heavy metals by solidification/stabilization of co-
536 disposed flue gas desulfurization brine and coal fly ash. *Energy Fuels* **30**, 5042–5051 (2016).

537   13.   Okoronkwo, M. U., Balonis, M., Katz, L., Juenger, M. & Sant, G. A thermodynamics-based
538   approach for examining the suitability of cementitious formulations for solidifying and
539   stabilizing coal-combustion wastes. *Journal of Environmental Management* **217**, 278–287
540   (2018).
541   14.   Kogbara, R. B., Al-Tabbaa, A. & Stegemann, J. A. Comparisons of operating envelopes for
542   contaminated soil stabilised/solidified with different cementitious binders. *Environ. Sci. Pollut.*
543   *Res.* **21**, 3395–3414 (2014).
544   15.   U.S. EPA (Environmental Protection Agency). *Waste and Materials - Flow Benchmark*
545   *Sector Report: Beneficial Use of Secondary Materials - Coal Combustion Products*. 95 (2008).
546   16.   Ellison, K. Brine-Encapsulation Bench & Field Testing Recommendations. in (2017).
547   17.   Feng, P., Miao, C. & Bullard, J. W. Factors Influencing the Stability of AFm and AFt in the
548   Ca-Al-S-O-H System at 25 °C. *J. Am. Ceram. Soc.* **99**, 1031–1041 (2016).
549   18.   Christensen, A. N., Jensen, T. R. & Hanson, J. C. Formation of ettringite,
550     $Ca_6Al_2(SO_4)_3(OH)_{12} \cdot 26H_2O$, AFt, and monosulfate, $Ca_4Al_2O_6(SO_4) \cdot 14H_2O$, AFm-14, in
551   hydrothermal hydration of Portland cement and of calcium aluminum oxide—calcium sulfate
552   dihydrate mixtures studied by in situ synchrotron X-ray powder diffraction. *Journal of Solid*
553   *State Chemistry* **177**, 1944–1951 (2004).
554   19.   Rajasekaran, G. Sulphate attack and ettringite formation in the lime and cement
555   stabilized marine clays. *Ocean Engineering* **32**, 1133–1159 (2005).
556   20.   Balonis, M., Lothenbach, B., Le Saout, G. & Glasser, F. P. Impact of chloride on the
557   mineralogy of hydrated Portland cement systems. *Cement and Concrete Research* **40**, 1009–
558   1022 (2010).
559   21.   Mesbah, A. *et al.* Crystal structure of Kuzel's salt $3CaO \cdot Al_2O_3 \cdot 1/2CaSO_4 \cdot 1/2CaCl_2 \cdot 11H_2O$
560   determined by synchrotron powder diffraction. *Cement and Concrete Research* **41**, 504–509
561   (2011).
562   22.   Jeon, D., Yum, W. S., Jeong, Y. & Oh, J. E. Properties of quicklime (CaO)-activated Class F
563   fly ash with the use of $CaCl_2$. *Cement and Concrete Research* **111**, 147–156 (2018).
564   23.   Glasser, F. P., Kindness, A. & Stronach, S. A. Stability and solubility relationships in AFm
565   phases Part I. Chloride, sulfate and hydroxide. *Cement and Concrete Research* **29**, 861–866
566   (1999).
567   24.   Birnin-Yauri, U. A. & Glasser, F. P. Friedel's salt, $Ca_2Al(OH)_6(Cl,OH) \cdot 2H_2O$: its solid
568   solutions and their role in chloride binding. *Cement and Concrete Research* **28**, 1713–1723
569   (1998).
570   25.   Hirao, H., Yamada, K., Takahashi, H. & Zibara, H. Chloride binding of cement estimated
571   by binding isotherms of hydrates. *Journal of Advanced Concrete Technology* **3**, 77–84 (2005).
572   26.   Gégout, P., Revertégat, E. & Moine, G. Action of chloride ions on hydrated cement
573   pastes: Influence of the cement type and long time effect of the concentration of chlorides.
574   *Cement and Concrete Research* **22**, 451–457 (1992).
575   27.   Beaudoin, J. J., Ramachandran, V. S. & Feldman, R. F. Interaction of chloride and C-S-H.
576   *Cement and Concrete Research* **20**, 875–883 (1990).
577   28.   Collin, M. *et al.* Fly Ash–$Ca(OH)_2$ Reactivity in Hypersaline NaCl and $CaCl_2$ Brines. *ACS*
578   *Sustainable Chem. Eng.* **9**, 8561–8571 (2021).

579   29.   Chancey, R. T., Stutzman, P., Juenger, M. C. G. & Fowler, D. W. Comprehensive phase
580   characterization of crystalline and amorphous phases of a Class F fly ash. *Cement and Concrete*
581   *Research* **40**, 146–156 (2010).
582   30.   Durdziński, P. T., Dunant, C. F., Haha, M. B. & Scrivener, K. L. A new quantification
583   method based on SEM-EDS to assess fly ash composition and study the reaction of its individual
584   components in hydrating cement paste. *Cement and Concrete Research* **73**, 111–122 (2015).
585   31.   Oey, T. *et al.* An improved basis for characterizing the suitability of fly ash as a cement
586   replacement agent. *J Am Ceram Soc* **100**, 4785–4800 (2017).
587   32.   Oey, T. *et al.* The influence of water activity on the hydration rate of tricalcium silicate. *J.*
588   *Am. Ceram. Soc.* **99**, 2481–2492 (2016).
589   33.   Lothenbach, B., Durdziński, P. T. & De Weerdt, K. Thermogravimetric analysis. in *A*
590   *practical guide to Microstructural analysis of cementitious materials* (2016).
591   34.   Shi, Z. *et al.* Friedel's salt profiles from thermogravimetric analysis and thermodynamic
592   modelling of Portland cement-based mortars exposed to sodium chloride solution. *Cement and*
593   *Concrete Composites* **78**, 73–83 (2017).
594   35.   Doebelin, N. & Kleeberg, R. Profex: a graphical user interface for the Rietveld refinement
595   program BGMN. *J Appl Crystallogr* **48**, 1573–1580 (2015).
596   36.   Rietveld, H. M. A profile refinement method for nuclear and magnetic structures. *J Appl*
597   *Crystallogr* **2**, 65–71 (1969).
598   37.   Bergmann, J., Friedel, P. & Kleeberg, R. BGMN - a new fundamental parameters based
599   Rietveld program for laboratory X-ray sources, it's use in quantitative analysis and structure
600   investigations. *Commission on Powder Diffraction (IUCr)* **20**, 5–8 (1998).
601   38.   Li, G., Le Bescop, P. & Moranville-Regourd, M. Synthesis of the U phase
602   (4CaO·0.9Al$_2$O$_3$·1.1SO$_3$·0.5Na$_2$O·16H$_2$O). *Cement and Concrete Research* **27**, 7–13 (1997).
603   39.   Kulik, D. A. *et al.* GEM-Selektor geochemical modeling package: revised algorithm and
604   GEMS3K numerical kernel for coupled simulation codes. *Comput Geosci* (2012)
605   doi:10.1007/s10596-012-9310-6.
606   40.   Wagner, T., Kulik, D. A., Hingerl, F. F. & Dmytrieva, S. V. GEM-Selektor geochemical
607   modeling package: TSolMod library and data interface for multicomponent phase models. *The*
608   *Canadian Mineralogist* **50**, 1173–1195 (2012).
609   41.   Lothenbach, B., Matschei, T., Möschner, G. & Glasser, F. P. Thermodynamic modelling of
610   the effect of temperature on the hydration and porosity of Portland cement. *Cement and*
611   *Concrete Research* **38**, 1–18 (2008).
612   42.   Lothenbach, B. *et al.* Cemdata18: A chemical thermodynamic database for hydrated
613   Portland cements and alkali-activated materials. *Cement and Concrete Research* **115**, 472–506
614   (2019).
615   43.   Thoenen, T., Hummel, W., Berner, U. & Curti, E. *The PSINagra chemical thermodynamic*
616   *database 12/07.* (2014).
617   44.   Johnson, J. W., Oelkers, E. H. & Helgeson, H. C. SUPCRT92: A software package for
618   calculating the standard molal thermodynamic properties of minerals, gases, aqueous species,
619   and reactions from 1 to 5000 bar and 0 to 1000 °C. *Computers & Geosciences* **18**, 899–947
620   (1992).
621   45.   Hummel, W., Berner, U., Curti, E., Pearson, F. J. & Thoenen, T. Nagra/PSI Chemical
622   Thermodynamic Data Base 01/01. *Radiochimica Acta* **90**, (2002).

623   46.   Helgeson, H. C., Kirkham, D. H. & Flowers, G. C. Theoretical prediction of the
624   thermodynamic behavior of aqueous electrolytes by high pressures and temperatures; IV,
625   Calculation of activity coefficients, osmotic coefficients, and apparent molal and standard and
626   relative partial molal properties to 600 degrees C and 5kb. *American Journal of Science* **281**,
627   1249–1516 (1981).

628   47.   Vollpracht, A., Lothenbach, B., Snellings, R. & Haufe, J. The pore solution of blended
629   cements: a review. *Mater Struct* **49**, 3341–3367 (2016).

630   48.   Pitzer, K. S. Ion interaction approach: theory and data correlation. in *Activity Coefficients*
631   *in Electrolyte Solutions* 75–153 (CRC Press, 1991).

632   49.   Langmuir, D. *Aqueous environmental geochemistry*. (1998).

633   50.   Elakneswaran, Y., Owaki, E. & Nawa, T. Modelling Long-Term Durability Performance of
634   Cementitious Materials under Sodium Sulphate Interaction. *Applied Sciences* **8**, 2597 (2018).

635   51.   Lothenbach, B. & Gruskovnjak, A. Hydration of alkali-activated slag: thermodynamic
636   modelling. *Advances in Cement Research* **19**, 81–92 (2007).

637   52.   Blanc, P. *et al.* Modeling hydration of mine tailings: Production of hydraulic binders from
638   alkali-activated materials. *Cement and Concrete Research* **137**, 106216 (2020).

639   53.   Hazen, R. M. A useful fiction: polyhedral modeling of mineral properties. *American*
640   *Journal of Science* **288**, 242–269 (1988).

641   54.   Chermak, J. A. & Rimstidt, J. D. Estimating the free energy of formation of silicate
642   minerals at high temperatures from the sum of polyhedral contributions. *American*
643   *Mineralogist* **75**, 1376–1380 (1990).

644   55.   Zhen-Wu, B. Y. *et al.* zeo19: A thermodynamic database for assessing zeolite stability
645   during the corrosion of nuclear waste immobilization glasses. *npj Mater Degrad* **4**, 2 (2020).

646   56.   Dosch, W. & zur Strassen, H. Ein alkalihaltiges Calciumaluminatsulfathydrat (Natrium-
647   Monosulfat) / An alkali-containing calcium aluminate sulphate hydrate. *Zement-Kalk-Gips* **9**, 11
648   (1967).

649   57.   Li, G., Le Bescop, P. & Moranville, M. Expansion mechanism associated with the
650   secondary formation of the U phase in cement-based systems containing high amounts of
651   Na2SO4. *Cement and Concrete Research* **26**, 195–201 (1996).

652   58.   Li, G., Le Bescop, P. & Moranville, M. The U phase formation in cement-based systems
653   containing high amounts of Na2SO4. *Cement and Concrete Research* **26**, 27–33 (1996).

654   59.   Song, Y. *et al.* Machine learning enables rapid screening of reactive fly ashes based on
655   their network topology. *ACS Sustainable Chem. Eng.* **9**, 2639–2650 (2021).

656   60.   Bauchy, M. Topological Constraint Theory and Rigidity of Glasses. in *21st Century*
657   *Nanoscience – A Handbook* (ed. Sattler, K. D.) 13-1-13–20 (CRC Press, 2019).
658   doi:10.1201/9780367333003-13.

659   61.   Kapeluszna, E., Kotwica, Ł., Różycka, A. & Gołek, Ł. Incorporation of Al in C-A-S-H gels
660   with various Ca/Si and Al/Si ratio: Microstructural and structural characteristics with DTA/TG,
661   XRD, FTIR and TEM analysis. *Construction and Building Materials* **155**, 643–653 (2017).

662   62.   Bernard, E., Lothenbach, B., Le Goff, F., Pochard, I. & Dauzères, A. Effect of magnesium
663   on calcium silicate hydrate (C-S-H). *Cement and Concrete Research* **97**, 61–72 (2017).

664   63.   Matschei, T., Lothenbach, B. & Glasser, F. P. The AFm phase in Portland cement. *Cement*
665   *and Concrete Research* **37**, 118–130 (2007).

666   64.   Matschei, T., Lothenbach, B. & Glasser, F. P. Thermodynamic properties of Portland
667   cement hydrates in the system $CaO–Al_2O_3–SiO_2–CaSO_4–CaCO_3–H_2O$. *Cement and Concrete*
668   *Research* **37**, 1379–1410 (2007).
669   65.   Warren, C. J. & Reardon, E. J. The solubility of ettringite at 25 °C. *Cement and Concrete*
670   *Research* **24**, 1515–1524 (1994).
671   66.   Bothe, J. V. & Brown, P. W. PhreeqC modeling of Friedel's salt equilibria at 23±1 °C.
672   *Cement and Concrete Research* **34**, 1057–1063 (2004).
673   67.   Allada, R. K., Pless, J. D., Nenoff, T. M. & Navrotsky, A. Thermochemistry of Hydrotalcite-
674   like Phases Intercalated with CO_3^{2-}, NO_3^-, Cl^-, I^-, and ReO_4^-. *Chem. Mater.* **17**, 2455–2459 (2005).
675   68.   Bontchev, R. P., Liu, S., Krumhansl, J. L., Voigt, J. & Nenoff, T. M. Synthesis,
676   Characterization, and Ion Exchange Properties of Hydrotalcite $Mg_6Al_2(OH)_{16}(A)_x(A')_{2-x}·4H_2O$ (A,
677   A' = Cl^-, Br^-, I^-, and NO_3^-, $2 \geq x \geq 0$) Derivatives. *Chem. Mater.* **15**, 3669–3675 (2003).
678   69.   Ke, X., Bernal, S. A. & Provis, J. L. Uptake of chloride and carbonate by Mg-Al and Ca-Al
679   layered double hydroxides in simulated pore solutions of alkali-activated slag cement. *Cement*
680   *and Concrete Research* **100**, 1–13 (2017).
681   70.   Cavani, F., Trifirò, F. & Vaccari, A. Hydrotalcite-type anionic clays: Preparation,
682   properties and applications. *Catalysis Today* **11**, 173–301 (1991).
683   71.   Balonis, M. The Influence of Inorganic Chemical Accelerators and Corrosion Inhibitors on
684   the Mineralogy of Hydrated Portland Cement Systems'. (Aberdeen University, 2010).
685   72.   Collin, M. *et al.* Fly ash degree of reaction in hypersaline NaCl and $CaCl_2$ brines: effects of
686   calcium-based additives. *Prepared for Submission to ACS Sustainable Chemistry & Engineering*.
687   73.   La Plante, E. C. *et al.* Enhancing silicate dissolution kinetics in hyperalkaline
688   environments. *J. Phys. Chem. C* **123**, 3687–3695 (2019).
689   74.   Brady, P. V. & Walther, J. V. Controls on silicate dissolution rates in neutral and basic pH
690   solutions at 25°C. *Geochimica et Cosmochimica Acta* **53**, 2823–2830 (1989).
691   75.   Oelkers, E. H. & Schott, J. The effect of aluminum, pH, and chemical affinity on the rates
692   of aluminosilicate dissolution reactions. *Geochimica et Cosmochimica Acta* **58**, 2011–2024
693   (1994).
694   76.   Fournier, M., Frugier, P. & Gin, S. Resumption of alteration at high temperature and pH:
695   rates measurements and comparison with initial rates. *Procedia Materials Science* **7**, 202–208
696   (2014).
697
698

699 **SUPPLEMENTARY INFORMATION**

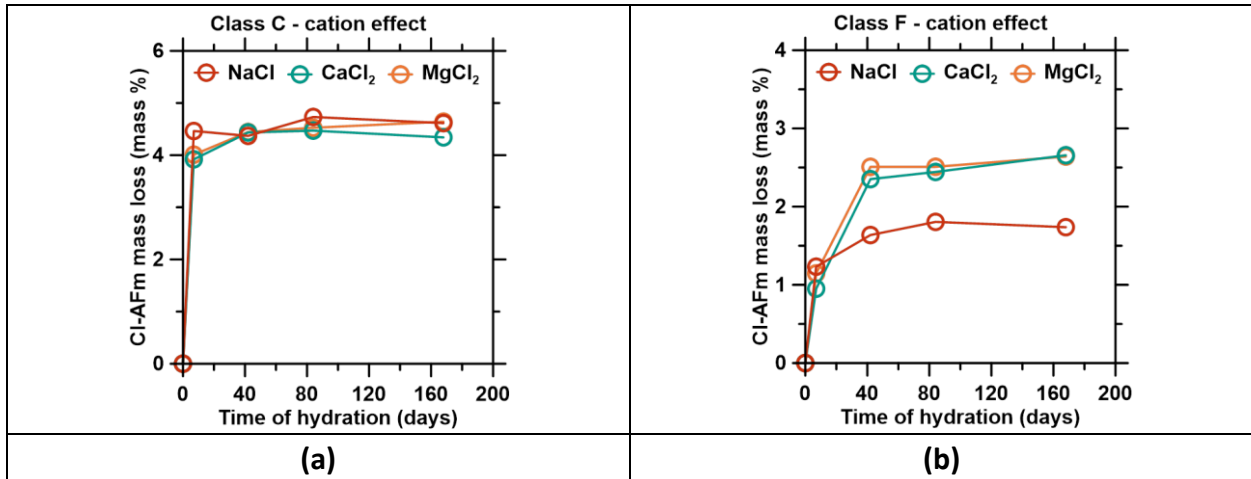700 *Single-salt brines*

701

(a)

(b)

Figure S1. The Cl-AFm phases mass loss – as measured by TGA – from 7 to 168 days of hydration at 25 °C for **(a)** the Class C fly ash in single-salt brines, and **(b)** for the Class F fly in single-salt brines.
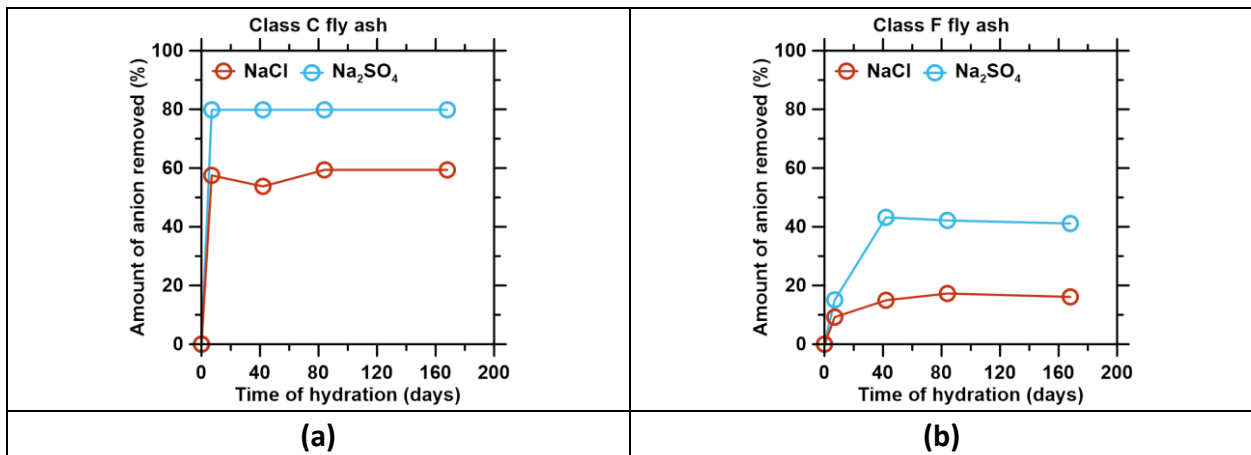
702

(a)

(b)

Figure S2. The amount of anion (Cl$^-$ or SO$_4^{2-}$) removed from the pore solution from 7 to 168 days of hydration at 25 °C **(a)** the Class C fly ash in single-salt brines, and **(b)** for the Class F fly in single-salt brines.
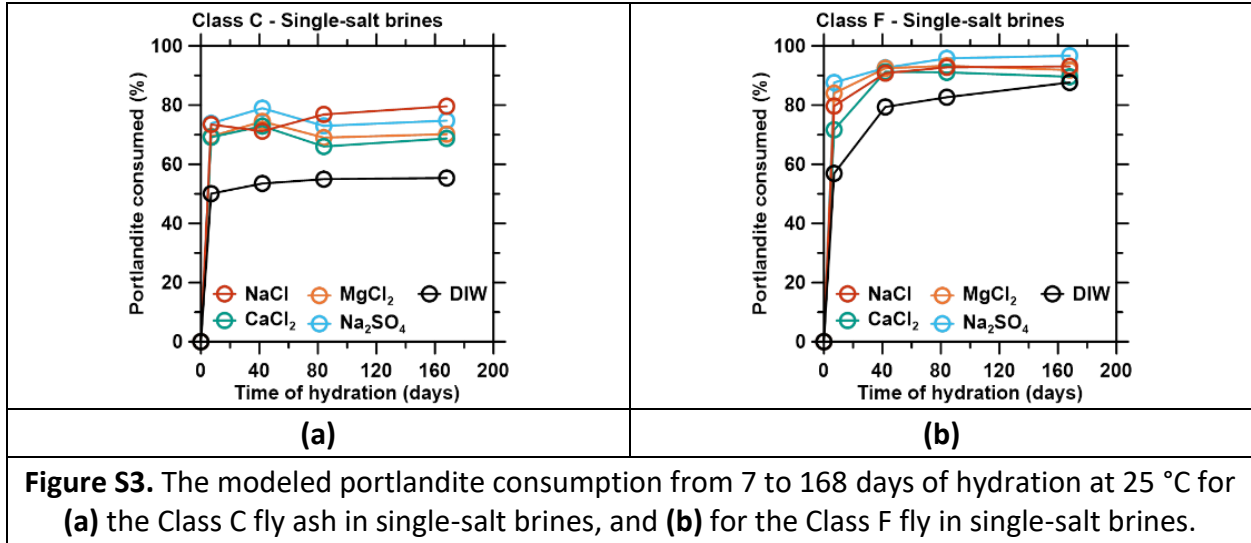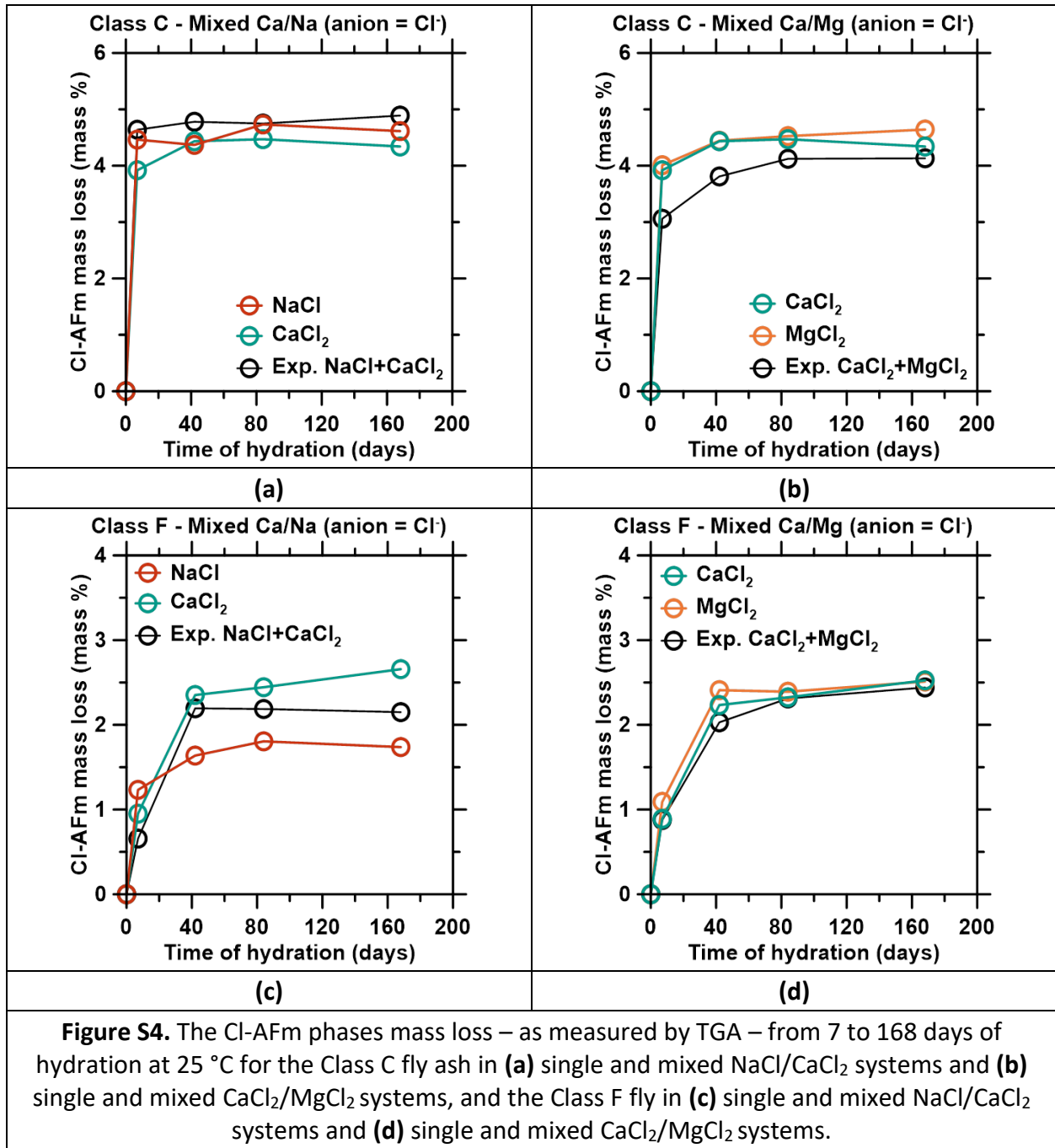
703

| (a) | (b) |

Figure S3. The modeled portlandite consumption from 7 to 168 days of hydration at 25 °C for **(a)** the Class C fly ash in single-salt brines, and **(b)** for the Class F fly in single-salt brines.
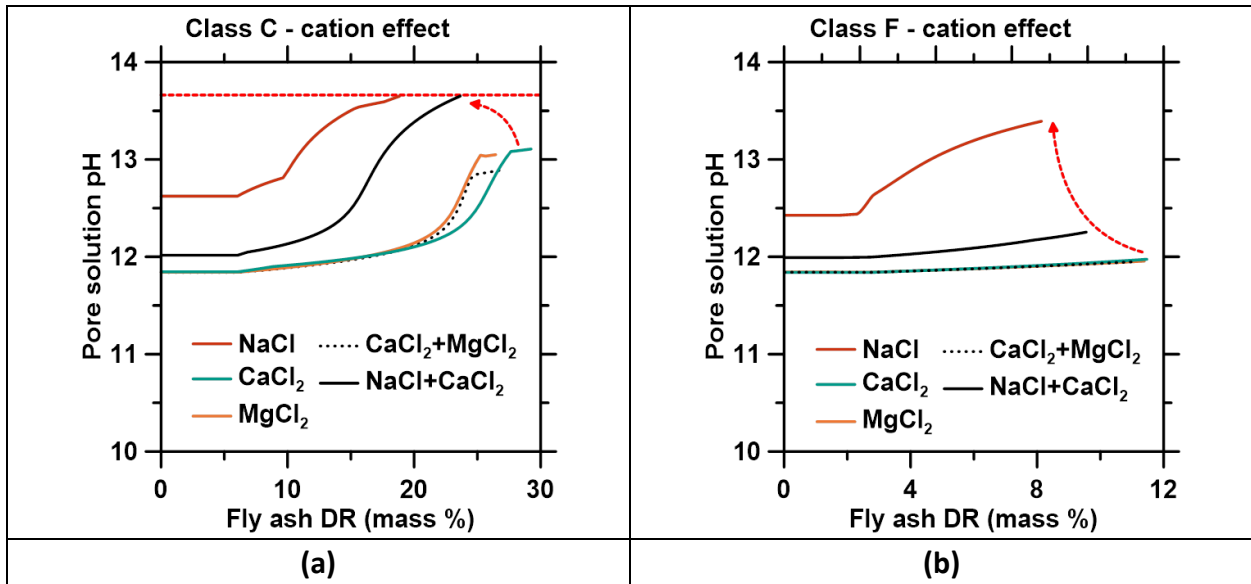
704

705   *Mixed-salt brines*

706

Figure S4. The Cl-AFm phases mass loss – as measured by TGA – from 7 to 168 days of hydration at 25 °C for the Class C fly ash in **(a)** single and mixed $NaCl/CaCl_2$ systems and **(b)** single and mixed $CaCl_2/MgCl_2$ systems, and the Class F fly in **(c)** single and mixed $NaCl/CaCl_2$ systems and **(d)** single and mixed $CaCl_2/MgCl_2$ systems.

707

Figure S5. The modeled pH of the pore solution as a function of the fly ash degree of reaction for **(a)** the Class C fly ash and **(b)** the Class F fly. The red line indicates the pH threshold after which the Class C fly ash stops reacting. The red arrows are a visual guideline showing the trend of decreasing fly ash DR with increasing pH.
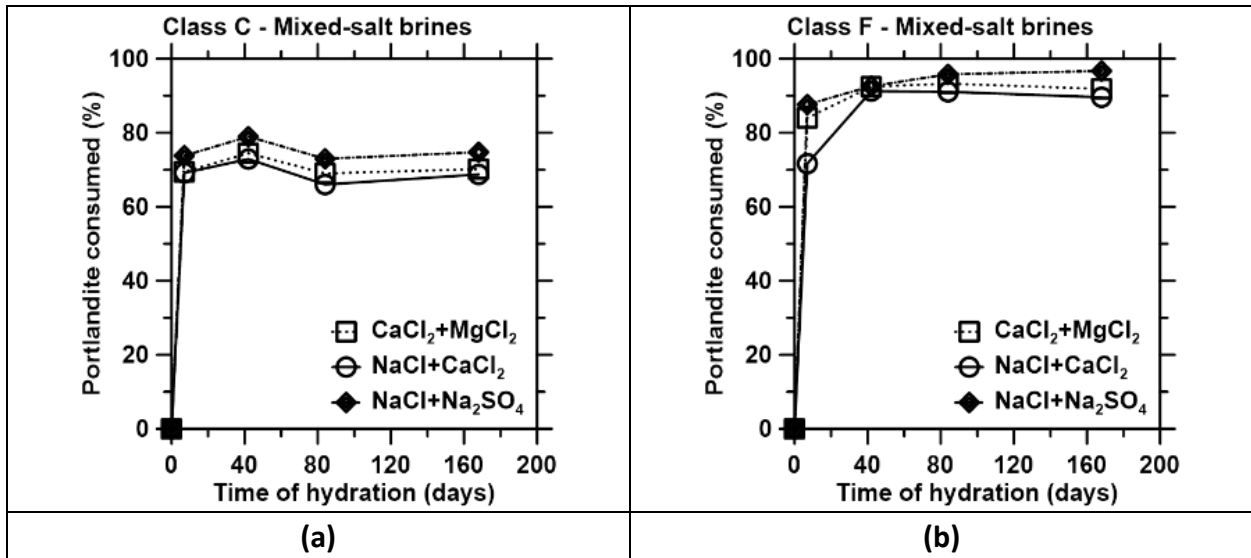
708

Figure S6. The modeled portlandite consumption from 7 to 168 days of hydration at 25 °C for **(a)** the Class C fly ash in mixed-salt brines, and **(b)** for the Class F fly in mixed-salt brines.

709